PROCEEDINGS OF SCIENCE

Magnetic field line path length variations and effects on solar energetic particle transport

David Ruffolo,[a,*] **Wirin Sonsrettee,**[b] **Piyanate Chuychai,**[c] **Achara Seripienlert,**[d] **Paisan Tooprakai,**[e] **Alejandro Sáiz,**[a] **William H. Matthaeus**[f,g] **and Rohit Chhiber**[f,h]

[a] *Department of Physics, Faculty of Science, Mahidol University, Bangkok, Thailand*
[b] *Faculty of Engineering and Technology, Panyapiwat Institute of Management, Nonthaburi, Thailand*
[c] *33/5 Moo 16, Tambon Bandu, Muang District, Chiang Rai, Thailand*
[d] *National Astronomical Research Institute of Thailand (NARIT), Chiang Mai, Thailand*
[e] *Department of Physics, Faculty of Science, Chulalongkorn University, Bangkok, Thailand*
[f] *Department of Physics and Astronomy, University of Delaware, Newark, DE, USA*
[g] *Bartol Research Institute, University of Delaware, Newark, DE, USA*
[h] *Heliophysics Science Division, NASA Goddard Space Flight Center, Greenbelt, MD, USA*

E-mail: david.ruf@mahidol.ac.th

Modeling of time profiles of solar energetic particle (SEP) observations typically considers transport along a large-scale magnetic field with a fixed path length from the source to the observer. Here we point out that variability in the turbulent field line path length can affect the fits to SEP data and the inferred mean free path and injection profile. To explore such variability, we perform Monte Carlo simulations in representations of homogeneous 2D MHD + slab turbulence in spherical geometry and trace trajectories of field lines and full particle orbits, considering proton injection from a narrow or wide angular region near the Sun, corresponding to an impulsive or gradual solar event, respectively. We analyze our simulation results in terms of path length statistics within and among $1^\circ \times 1^\circ$ pixels in heliolatitude and heliolongitude at 0.35 and 1 AU from the Sun. Field line path lengths relate to the fluctuation amplitudes experienced by the field lines, which in turn relate to the local topology of 2D turbulence. There are also systematic patterns in the peak path lengths of energetic particles arriving at different locations, because of variations in the underlying magnetic field line path lengths and variations in the pitch angle scattering experienced by the particles. We describe the effects of such path length variations on observed SEP time profiles, both in terms of path length variability at specific locations and motion of the observer with respect to turbulence topology during the course of the observations.

38th International Cosmic Ray Conference (ICRC2023)
26 July - 3 August, 2023
Nagoya, Japan

*Speaker

PoS(ICRC2023)1245

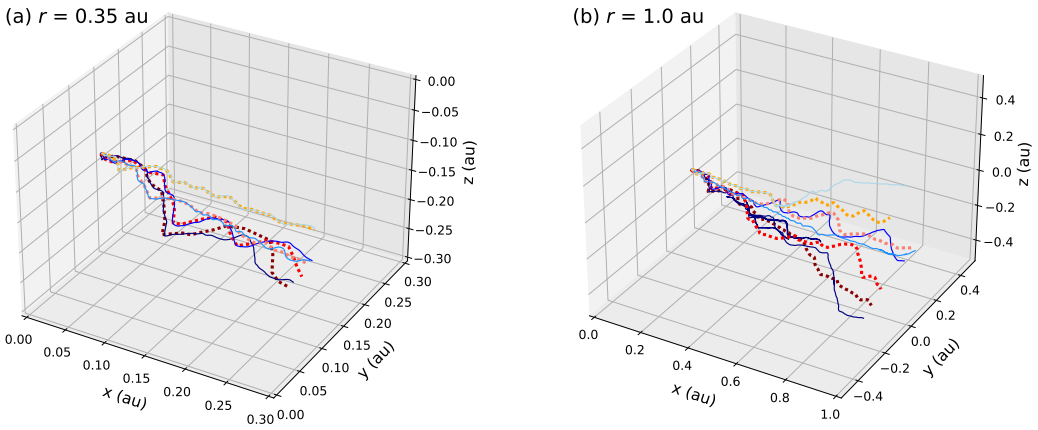

Figure 1: Illustration of sample 1 MeV proton trajectories (solid lines) and their associated field line trajectories (dashed lines) from the same initial location, based on full-orbit simulations in a representation of the 2D+slab model interplanetary turbulence with normalized rms magnetic fluctuation $b/B_0 = 1$ and slab fraction $f_s = 0.2$. (a) The trajectories are traced to $r = 0.35$ au from the Sun. We can see that the particles mostly closely follow the field lines. (b) But when we extend them to $r = 1$ au, more deviation between particle and field line trajectories can be observed. While each particle is no longer closely following its original field line, statistically we find that the path lengths and lateral spread of particles are closely related to those of field lines. Effects of particle backscattering can also be seen.

1. Introduction

The interplanetary transport of SEPs, including scattering due to magnetic fluctuations in the solar wind, typically plays a dominant role in determining their intensity and anisotropy profiles, which are a key aspect of space weather effects of solar storms. SEP trajectories can be considered to be determined by those of the magnetic field lines combined with the effect of parallel scattering [1], as indicated in Figure 1 based on full-orbit simulations of sample particle and field line trajectories in a representation of interplanetary turbulence. Because of this close relation between field line and particle trajectories, models of SEP time profiles typically consider transport along a large-scale magnetic field with a fixed path length from the source to the observer.

Observationally, velocity dispersion analysis is applied to an onset time t for various particle energy channels, each with a corresponding a particle velocity v, which are fit to an equation $t = t_{\rm start} + s/v$, where $t_{\rm start}$ is interpreted as the start time of injection. A common interpretation is that scattering effects can be neglected for first-arriving particles, so s is interpreted as the path length along the large-scale guiding magnetic field. However, it has been pointed out that more generally, if scattering is not neglected, s should be interpreted as the path length of initially arriving particle orbits, including their gyration around the magnetic field. Various studies have suggested that the scattering effects should not be neglected [2, 3], including a recent analysis of SEP ions observed using the *Parker Solar Probe* (PSP), from which $s \approx 0.625$ au was inferred at a radial distance of $r \approx 0.35$ au from the Sun [4]. In this case it seems particularly unlikely that s represents the path length of the large-scale interplanetary magnetic field; rather the difference between $s = 0.625$ and $r = 0.35$ was attributed to a combination of the enhanced path length of random-walking magnetic fields and scattering of the ions at the observed onset time to a typical

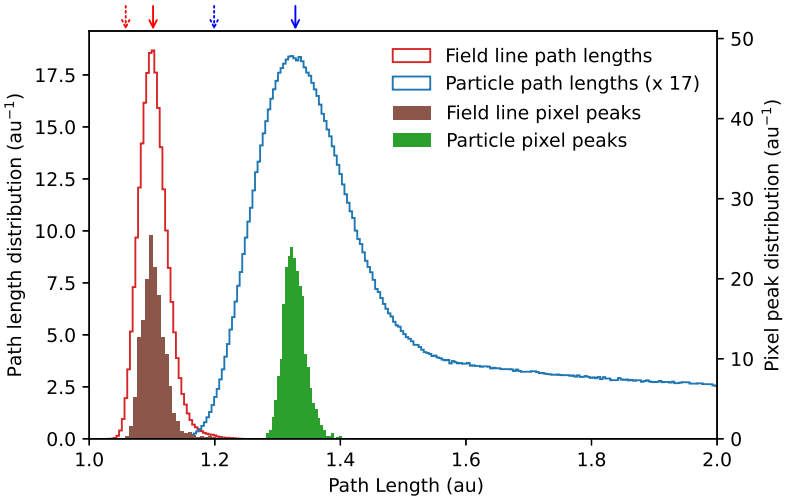

Figure 2: Path length distributions at $r = 1$ au from a simulation of 5 million sets of field lines (red) and 1 MeV protons (blue) for a wide injection region (as for a gradual SEP event) with $b/B_0 = 0.5$ and $f_s = 0.2$. Most probable ("peak") path lengths are indicated by solid arrows and 10% of peak by dashed arrows. For an instantaneous particle injection, the particle path length distribution would correspond to a time-intensity profile. Distributions of peak path lengths within "pixels" of $1° \times 1°$ in heliolatitude and heliolongitude for the field lines (brown) and particles (green) indicate the spatial variation of peak path lengths.

pitch angle of 25°. Based on full-orbit simulations of proton trajectories in a representation of interplanetary turbulence, it was found that the mean path length of guiding center trajectories of energetic particles was slightly shorter than that of the random-walking field lines, but full-orbit path lengths s were significantly longer, because the pitch angle is non-zero due to interplanetary scattering.

Here we extend the work of [4] to examine distributions and spatial variations in field line and particle path lengths. Figure 2 shows an example of how we characterize global distributions from Monte Carlo simulations of path lengths of field lines (red) and particles (blue), to any heliolongitude and heliolatitude at the distance r of interest, in terms of the most probable ("peak") path lengths (solid arrows) and path lengths to 10% of the peak (dashed arrows). For an instantaneous injection near the Sun, the particle path length distribution would directly correspond to a time-intensity profile of SEPs. To examine spatial variations, we divide heliolongitudes and heliolatitudes into $1° \times 1°$ "pixels," allowing us to construct maps of the peak path length of field lines or particles arriving at each pixel; distributions of these peak values are also shown in Figure 2 (solid histograms).

2. Methods

The simulation of magnetic turbulence in the solar wind is based on a idealized two-component fluctuation model with slab and 2D components, motivated by observations of a "Maltese cross" pattern of solar wind magnetic fluctuations varying predominantly in directions parallel or perpendicular to the mean field, respectively [5, 6]. As expressed in spherical geometry, the 2D+slab

model would ideally have the form [7, 8]

$$\mathbf{B}\,(\mathbf{r}) = \mathbf{B}_0\,(\mathbf{r}) + \mathbf{b}(\mathbf{r}) = \frac{r_1^2}{r^2}\left[B_1\hat{\mathbf{r}} + \mathbf{b}^{\rm slab}\,(r) + \mathbf{b}^{\rm 2D}\,(\varphi,\Lambda)\right]. \quad (1)$$

A radial mean field was used in order to allow the construction of a statistically homogeneous 2D fluctuation field, $\mathbf{b}^{\rm 2D}(\varphi,\Lambda)$, that depends only on the heliolongitude φ and heliolatitude Λ.

The total magnetic field $\mathbf{B}$ is proportional to r^{-2} and the magnitude of the radial mean magnetic field $\mathbf{B_0}$ is $B_1 = 5$ nT at $r_1 = 1$ au. The two components of the fluctuation model are the slab fluctuation $\mathbf{b}^{\rm slab}$, and the 2D fluctuation $\mathbf{b}^{\rm 2D}$, which are perpendicular to the mean field. For simplicity, the fluctuation amplitude relative to the mean field is taken to be independent of r, although PSP observations indicate that it actually varies as $r^{1/4}$ inside Earth orbit [9]. The 2D component $\mathbf{b}^{\rm 2D}$ depends on the perpendicular coordinates: φ and Λ. In order to generate more realistic 2D fluctuations with coherent structures, we use a 2D magnetohydrodynamic (MHD) simulation [8]. The 2D magnetic potential is then mapped from Cartesian coordinates (x, y) to angular coordinates (φ,Λ), with the total 2D correlation scale set to $\lambda_{c2} = 0.0123$ au, similar to the value measured by [10], neglecting the mild variation inferred from PSP data [11]. Similarly, the slab fluctuation field $\mathbf{b}^{\rm slab}$ is generated along one dimension, z, from a turbulence power spectrum with the bendover scale 0.02 au and an inertial range with a Kolmogorov spectrum [8]. When mapping onto angular coordinates, in order to maintain $\nabla\cdot\mathbf{b}^{\rm slab} = 0$, we need to modify Equation (1) to use $b_\varphi^{\rm slab}(r) = b_x^{\rm slab}(z)$ and $b_\Lambda^{\rm slab}(r,\Lambda) = b_y^{\rm slab}(z)\sec\Lambda$. To some degree, this violates homogeneity, but we use a simulation domain of $-25^\circ \le \varphi \le 25^\circ$ and $-25^\circ \le \Lambda \le 25^\circ$, so the factor of $\sec\Lambda$ has only a minor effect.

To investigate the variations of path lengths of solar energetic particles (SEPs), we use a Monte Carlo approach, tracing field lines and particles from either a narrow or wide injection region at $r = 0.1$ au, corresponding to an impulsive or gradual solar particle event, respectively. For a narrow injection, we randomly inject magnetic field lines and particles within a 5°-diameter circle centered at $\varphi = \Lambda = 0$ [8]. In this case we do not use periodic boundary conditions in φ and Λ, and trajectory tracing is terminated if a field line or particle reaches those boundaries. To model a wide injection, we use uniformly random injection positions over the entire (φ,Λ) domain, with periodic boundary conditions in φ and Λ to efficiently model homogeneous injection from a wider range of angles [7].

The streamline equation is used to trace the trajectories of magnetic field lines in spherical geometry. For particle trajectories, we solve the Newton-Lorentz equation. Both field line and particle trajectories are traced numerically using a version of the STREAMLINE code [12]. The path length of a field line is evaluated as $S = S_0 + \int_{r_0}^{r}(dS/dr)dr$ [4] where S_0 represents the path length inside r_0, which we simply set to r_0 so that a radial field line with no turbulence has $S = r$. An analogous formula is used to calculate the path length s of a particle. Since we assume transverse fluctuations, for field lines we have $dS/dr = \sqrt{1 + b^2/B_0^2}$.

We record and analyze all crossings of field lines and particles at the spherical shells at distances $r_A = 0.35$ or $r_B = 1$ au from the Sun; for brevity, here we only discuss results for r_A. Unlike a real detector at a specific location in space, one spherical shell is sometimes traversed by a single particle many times. With a limited Monte Carlo sample, such a particle provides an excessively strong contribution to the path length distribution, so we retain at most 10 crossings by a single

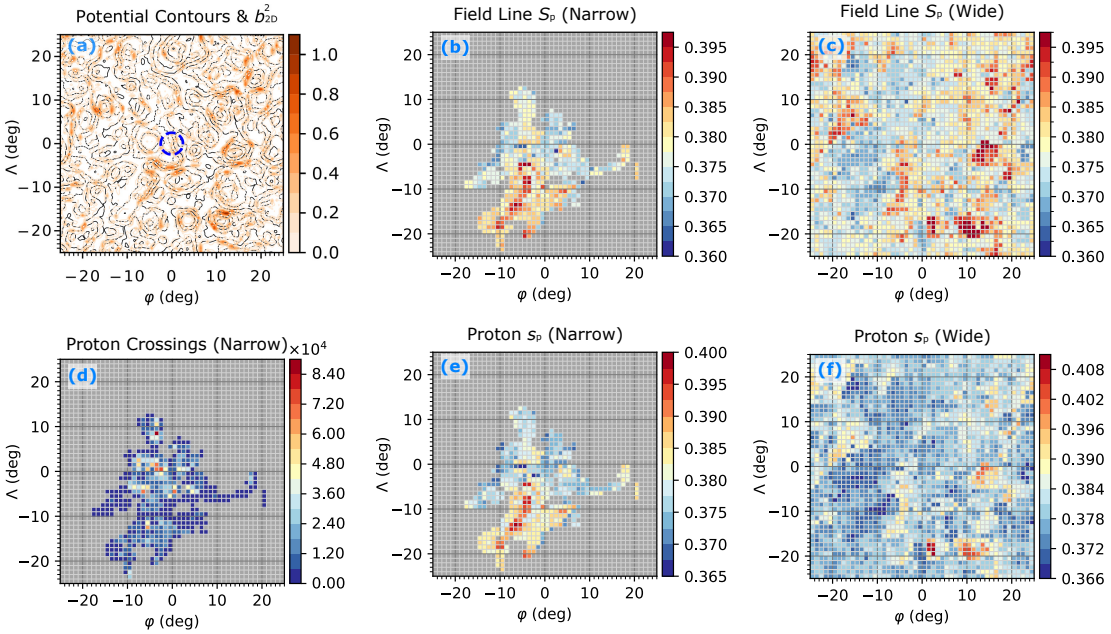

Figure 3: Maps in heliolongitude φ and heliolatitude Λ at radius $r_A = 0.35$ au, for turbulence parameters $b/B_0 = 0.5$ and $f_s = 0.2$: (a) Contours of equal magnetic potential $a(\Lambda, \varphi)$ and resulting $(b^{2D})^2$ (color scale). (b) Peak path length in each pixel of (Λ, φ) for field lines traced from a circle of radius 2.5° at $r_0 = 0.1$ au, to model the distribution of field lines connected to the narrow injection region of an impulsive solar event. (c) Like (b), for field lines traced from all locations at $r_0 = 0.1$ au, to model the distribution of field lines connected to the wide injection region of a gradual solar event. (d) Number of crossings at r_A in each angular pixel for 1 MeV protons traced from the narrow injection region. (e) Peak length for crossings of 1 MeV protons traced from the narrow injection region. (f) Like (e), but for the wide injection region. There are systematic variations in path length and arrival time that relate to the topology of 2D turbulence. The spatial pattern of peak proton path lengths closely follows that for field lines, which in turn have longer path lengths in pixels where (a) indicates a strong $\mathbf{b}^{2D}$.

particle. To examine the spatial variability of path lengths, we divide the domain of heliolongitude and heliolatitude into 2500 square-degree boxes, called "pixels."

We have developed an algorithm to fit path length distributions, possibly with as few as 70 path length values, to estimate the most probable ("peak") value. For spatial maps, in heliolongitude and heliolatitude, we plot only pixels with at least 70 crossings. Note that some pixels are essentially inaccessible to outward-moving particles, a phenomenon associated with SEP "dropouts" [13], and may have very long peak path lengths associated with backscattering particles. A detector at such a location would not register a strong SEP event. In our maps we exclude pixels with peak path length > 1.05 au, in order to focus on pixels with a significant population of outward-moving SEPs. In maps of the number of particle crossings, we also exclude crossings of path length > 0.41 au; if long path lengths were not excluded, the number of crossings due to backscattering would increase without bound for longer simulation durations.

3. Results and Discussion

Figure 3(a) shows a contour map of the magnetic potential $a(\varphi, \Lambda)$, used to generate $\mathbf{b}^{2D}(\varphi, \Lambda) = \nabla \times [a(\varphi, \Lambda)\hat{\mathbf{r}}]$, which then follows the equipotential contours. For a mean field with 2D fluctuations, the magnetic field lines would be forever trapped along such contours, representing an idealized flux tube ("spaghetti") structure [14, 15]. In our simulations we also add a slab component, so field lines experience only temporary topological trapping, giving rise to a dropout pattern [16]. For the results in this section, we use a turbulence amplitude of $b/B_0 = 0.5$ and slab fraction $f_s = 0.2$.

Figures 3(b-c) show the most probable ("peak") path length of field lines in each pixel, for a narrow or wide injection region, respectively. In either case, we see systematic variations that relate to $(b^{2D})^2$ *at the distance* r_A, as indicated by the red color scale (in units of B_0^2) in Figure 3(a). As noted earlier, the path length S of a field line is the integral of $dS/dr = \sqrt{1 + b^2/B_0^2}$ *over its entire trajectory*, so apparently $(b^{2D})^2$ at r_A serves as a proxy of $b^2 = (b^{2D})^2 + (b^{slab})^2$ over the trajectory. The minority slab contribution is nearly independent of (φ, Λ), so the path length variation pattern indicates that $(b^{2D})^2$ at r_A serves as a proxy of its value throughout the trajectories. In some regions, this reflects a topological trapping effect of confinement of field lines to "islands" of the 2D turbulence with closed field lines, and in other regions to (φ, Λ) trajectories that traverse long regions of strong $(b^{2D})^2$.

Figure 3(d) is a map of the number of 1 MeV proton crossings at 0.35 au in each pixel for the narrow injection region. This is the irregular dropout pattern as previously reported [8, 16–18], which actually has fine structure that has been coarse-grained at the 1° level in this pixel map. Interestingly, in this coarse-grained representation we observe a more centrally concentrated distribution at a distance of 1 au, presumably as a result of the central limit theorem for superposition of numerous random trajectory segments. For a wide injection, as appropriate for modeling a gradual solar event, the distribution of crossings is much more uniform as has been noted previously [7, 17].

Figures 3(e-f) show peak full-orbit path lengths of the protons arriving at each pixel, in analogy with Figures 3(b-c) for field lines. There is a striking similarity between the patterns for protons and for field lines, as the proton path lengths to 0.35 au are only slightly longer than those of field lines. These results are for a proton energy of 1 MeV, and we obtained qualitatively similar results for an energy of 25 MeV. Thus the spatial variation of SEP path lengths also bears the imprint of the 2D magnetic field pattern, which in turn relates to the flux-tube structure of the solar wind.

Path length variations include the spatial variations shown in Figure 3 as well as variation in terms of a distribution of path lengths of field lines and particles arriving at a location of interest, e.g., the location of a detector. Indeed, an observed time-intensity profile of SEPs from a near-solar source represents the distribution in path length s, converted to travel time $t = s/v$ and convoluted with the injection profile. In addition, SEP modeling should allow for field line path lengths S that are longer than that along the mean field (which in this work would be $S = r$) as previously described by theory and simulations [4], with some uncertainty due to the variation with heliolongitude and heliolatitude as described here, as well as unknown parameters of interplanetary turbulence. Therefore, the path length of the guiding field lines in a transport model could be treated as an adjustable parameter. As noted earlier, it is not appropriate to identify a field line path length S with the typical path length s of particles near onset as determined by velocity dispersion

analysis, as the latter is greater due to interplanetary scattering.

Another effect of the spatial variation of the path lengths on SEP transport is that during the course of an SEP event observation, the dropout pattern can be convected with the solar wind flow past the spacecraft; indeed this is generally considered to explain why the spatial pattern of magnetic connectivity can result in sharp time variations of dropouts in impulsive SEP events [13, 17]. Furthermore, this effect of changing magnetic connectivity causing sharp time variations has also been observed in some gradual SEP events [19, 20]. While this could reflect the different density of SEPs along different flux tubes, it is also affected by spatial variation in the path length distribution, which can suddenly shift the time-intensity profile of one location (one "pixel" in our work) relative to that in a neighboring location.

4. Acknowledgements

This research has been supported in Thailand by Thailand Science Research and Innovation (RTA6280002), by the National Science and Technology Development Agency (NSTDA) and National Research Council of Thailand (NRCT): High-Potential Research Team Grant Program (N42A650868), and from the NSRF via the Program Management Unit for Human Resources & Institutional Development, Research and Innovation (B37G660015). It was also supported by the Parker Solar Probe mission under the ISOIS project (contract NNN06AA01C) and a subcontract to University of Delaware from Princeton University (SUB0000165) and by the IMAP project through a Princeton subcontract (SUB0000317). Additional support is acknowledged from NASA under the LWS program (NNX17AB79G, 80NSSC22K1020), the HSR program (80NSSC18K1210 & 80NSSC18K1648), and the Helio PSP-GI program (80NSSC21K1765).

References

[1] J. Minnie, W.H. Matthaeus, J.W. Bieber, D. Ruffolo and R.A. Burger, *When do particles follow field lines?*, *J. Geophys. Res. Space Phys.* **114** (2009) A01102.

[2] J. Lintunen and R. Vainio, *Solar energetic particle event onset as analyzed from simulated data*, *Astron. Astrophys.* **420** (2004) 343.

[3] A. Sáiz, P. Evenson, D. Ruffolo and J.W. Bieber, *On the Estimation of Solar Energetic Particle Injection Timing from Onset Times near Earth*, *Astrophys. J.* **626** (2005) 1131.

[4] R. Chhiber, W.H. Matthaeus, C.M.S. Cohen, D. Ruffolo, W. Sonsrettee, P. Tooprakai et al., *Magnetic field line random walk and solar energetic particle path lengths. Stochastic theory and PSP/IS⊙IS observations*, *Astron. Astrophys.* **650** (2021) A26 [2011.08329].

[5] W.H. Matthaeus, M.L. Goldstein and D.A. Roberts, *Evidence for the presence of quasi-two-dimensional nearly incompressible fluctuations in the solar wind*, *J. Geophys. Res.* **95** (1990) 20673.

[6] J.W. Bieber, W.H. Matthaeus, C.W. Smith, W. Wanner, M.-B. Kallenrode and G. Wibberenz, *Proton and Electron Mean Free Paths: The Palmer Consensus Revisited*, *Astrophys. J.* **420** (1994) 294.

[7] D. Ruffolo, A. Seripienlert, P. Tooprakai, P. Chuychai and W.H. Matthaeus, *Squeezing of Particle Distributions by Expanding Magnetic Turbulence and Space Weather Variability*, *Astrophys. J.* **779** (2013) 74.

[8] P. Tooprakai, A. Seripienlert, D. Ruffolo, P. Chuychai and W.H. Matthaeus, *Simulations of Lateral Transport and Dropout Structure of Energetic Particles from Impulsive Solar Flares*, *Astrophys. J.* **831** (2016) 195.

[9] R. Chhiber, *Anisotropic Magnetic Turbulence in the Inner Heliosphere-Radial Evolution of Distributions Observed by Parker Solar Probe*, *Astrophys. J.* **939** (2022) 33 [2205.14096].

[10] J.M. Weygand, W.H. Matthaeus, S. Dasso, M.G. Kivelson, L.M. Kistler and C. Mouikis, *Anisotropy of the Taylor scale and the correlation scale in plasma sheet and solar wind magnetic field fluctuations*, *Journal of Geophysical Research (Space Physics)* **114** (2009) A07213.

[11] M.E. Cuesta, R. Chhiber, S. Roy, J. Goodwill, F. Pecora, J. Jarosik et al., *Isotropization and Evolution of Energy-containing Eddies in Solar Wind Turbulence: Parker Solar Probe, Helios 1, ACE, WIND, and Voyager 1*, *Astrophys. J. Lett.* **932** (2022) L11 [2205.00526].

[12] S. Dalena, P. Chuychai, R.L. Mace, A. Greco, G. Qin and W.H. Matthaeus, *Streamline generation code for particle dynamics description in numerical models of turbulence*, *Computer Physics Communications* **183** (2012) 1974.

[13] J.E. Mazur, G.M. Mason, J.R. Dwyer, J. Giacalone, J.R. Jokipii and E.C. Stone, *Interplanetary Magnetic Field Line Mixing Deduced from Impulsive Solar Flare Particles*, *Astrophys. J. Lett.* **532** (2000) L79.

[14] K.G. McCracken and N.F. Ness, *The Collimation of Cosmic Rays by the Interplanetary Magnetic Field*, *J. Geophys. Res.* **71** (1966) 3315.

[15] F. Mariani, B. Bavassano, U. Villante and N.F. Ness, *Variations of the occurrence rate of discontinuities in the interplanetary magnetic field*, *J. Geophys. Res.* **78** (1973) 8011.

[16] D. Ruffolo, W.H. Matthaeus and P. Chuychai, *Trapping of Solar Energetic Particles by the Small-Scale Topology of Solar Wind Turbulence*, *Astrophys. J. Lett.* **597** (2003) L169.

[17] J. Giacalone, J.R. Jokipii and J.E. Mazur, *Small-scale Gradients and Large-scale Diffusion of Charged Particles in the Heliospheric Magnetic Field*, *Astrophys. J. Lett.* **532** (2000) L75.

[18] G. Zimbardo, P. Pommois and P. Veltri, *Magnetic flux tube evolution in solar wind anisotropic magnetic turbulence*, *J. Geophys. Res. Space Phys.* **109** (2004) A02113.

[19] R.J. Nemzek, R.D. Belian, T.E. Cayton and G.D. Reeves, *The October 22, 1989, solar cosmic ray event measured at geosynchronous orbit*, *J. Geophys. Res.* **99** (1994) 4221.

[20] D. Ruffolo, P. Tooprakai, M. Rujiwarodom, T. Khumlumlert, M. Wechakama, J.W. Bieber et al., *Relativistic Solar Protons on 1989 October 22: Injection and Transport along Both Legs of a Closed Interplanetary Magnetic Loop*, *Astrophys. J.* **639** (2006) 1186.